



## Interfacial Behavior of Surface Activated p-GaP/n-GaAs Bonded Wafers at Room Temperature

M. M. R. Howlader,<sup>a,z</sup> T. Suga,<sup>b,\*</sup> F. Zhang,<sup>a</sup> T. H. Lee,<sup>c</sup> and M. J. Kim<sup>c</sup>

<sup>a</sup>Department of Electrical and Computer Engineering, McMaster University, Hamilton, Ontario L8S 4K1, Canada

<sup>b</sup>Department of Precision Engineering, University of Tokyo, Tokyo 113-8656, Japan

<sup>c</sup>Department of Materials Science and Engineering, University of Texas at Dallas, Texas 75080, USA

The interfacial behavior of the bonded p-GaP/n-GaAs wafers, with activated surfaces, that use an Ar fast atom beam was investigated. The bonding strength of the interface was 9.8 MPa at room temperature, and the GaP was fractured and remained on the GaAs following the tensile test. Two amorphous layers with identical thicknesses of 3.5 nm were found across the interface without annealing. When annealing was executed, the electrical current–voltage characteristics improved and the amorphous layers diminished across the interface. The amorphous layers adjacent to the GaP across the interface are attributed to the Ga-rich layer because of the depletion of P.

© 2009 The Electrochemical Society. [DOI: 10.1149/1.3272957] All rights reserved.

Manuscript submitted August 31, 2009; revised manuscript received November 17, 2009. Published December 17, 2009.

The integration of diverse combinations of III–V materials is required to create high speed/high frequency optoelectronic devices, such as light emitting diodes<sup>1</sup> and emitting lasers<sup>2</sup> with vertical cavity surfaces, on a single chip substrate. Epitaxial growth and direct wafer bonding methods have been developed to integrate III–V materials. For these integrations, lattice mismatch and coefficient of thermal expansion (CTE) are two major issues. For example, the lattice mismatch between GaP and GaAs is around 3.57%, and the CTEs for GaP and GaAs are  $5.91 \times 10^{-6}$  and  $6.63 \times 10^{-6}/^{\circ}\text{C}$ , respectively.<sup>2</sup> As a result, the lattice mismatch caused high density dislocations between the heteroepitaxial layers fabricated at high temperatures. Generally, thick buffer layers are used to reduce the dislocations; however, these are not desirable for optoelectronic device applications.<sup>3,4</sup> Wafer bonding at high temperatures may fracture the bonded interface of the GaP and GaAs because of the difference in CTE. Heating at high temperatures may not be acceptable for bonding wafers because other materials, such as metallic layers and polymer lenses,<sup>5</sup> have comparatively low melting points.

A room-temperature wafer bonding called surface activated bonding (SAB) has been implemented to bond the GaP and GaAs wafers. The SAB allows spontaneous bonding without annealing.<sup>6–8</sup> In this method, the wafer surfaces are activated by using an argon fast atom beam (Ar-FAB), and then the surfaces were bonded in an ultrahigh vacuum (UHV). The surface roughness of the activated surfaces had to be lower than 1 nm [root-mean-square (rms)] to achieve a spontaneous adhesion between the surfaces.<sup>6</sup> During surface activation, crystalline surfaces can change into amorphous layers because of sputtering and displacement damages. This may affect the characteristic behavior of the bonded interface.<sup>7,8</sup> While direct bonding mechanisms of different combinations of Si, GaAs, and InP have been reported,<sup>9–14</sup> bonding of GaP and GaAs wafers without heat has not been accomplished yet.<sup>1,2,15</sup> Although the SAB does not require heat to bond, the bonded wafers may go through annealing steps when fabricating a device. For example, protective and antireflective layers were created at 425°C on GaP/GaAs bonded surfaces.<sup>2</sup> Therefore, the influences annealing might have on the electrical, mechanical, and structural behaviors of the GaP/GaAs bonded wafers may be of great interest. This article investigates the surface activation, the roughness, and the influences annealing has on the interface behaviors by analyzing the bonding strength, electrical behavior, and nanostructural characteristics of GaP/GaAs.

Mirror-polished n-GaAs(100) and p-GaP(100) (15° off-orientation) with dimensions  $10 \times 10 \times 0.35$  mm and  $20 \times 20 \times 0.25$  mm, respectively, were used. The p-GaP specimen was transparent. The resistivities of p-GaP and n-GaAs were (2.0–4.9)

$\times 10^{-1}$  and  $(2.2–2.3) \times 10^{-3}$   $\Omega$  cm, respectively. The doping elements for p-GaP and n-GaAs were Zn and Si, respectively, and the carrier concentrations were  $8 \times 10^{17}$  and  $(1.2–1.3) \times 10^{18}$   $\text{cm}^{-3}$ , respectively. The bonding experiments were carried out using a flip-chip-based SAB equipment, which consisted of a two-load lock, a process, a transfer, an analysis, and a bonding chamber.<sup>6–8</sup> The specimens were cleaned with acetone and ethanol before they were loaded into the load lock chamber. The specimens were separately activated using 1.5 keV of Ar-FAB ions with a dose rate of  $2.38 \times 10^{14}$   $\text{i}/\text{cm}^2$  s in the processing chamber at a pressure of  $<10^{-6}$  Pa for 180 s. The wafers were bonded in the bonding chamber under an external force of 60 kgf for 60 s. The time that elapsed from activation to bonding was 23 min.

Ohmic and nonohmic contacts were made at the center of both sides to measure the current–voltage ( $I$ - $V$ ) behavior. For ohmic contacts, electrodes with 8 mm diameters were prepared on one side of the p-GaP specimen before bonding by depositing Zn followed by Au at room temperature. Then, the electrodes deposited on the p-GaP specimen were annealed at 500°C in a vacuum pressure of  $4 \times 10^{-4}$  Pa for 30 min to make an ohmic contact. The heating rate was 140°C/min. Sizes of electrodes similar to those of the p-GaP specimen were prepared on n-GaAs by the deposition of Ge followed by Au at room temperature. Then, the n-GaAs specimen was annealed at 400°C for 60 s with a heating rate of 90°C/min. The bonded specimens with ohmic electrodes were not annealed. To avoid heating influence on bonded and annealed specimens resulting from processing temperatures for ohmic electrodes, the ohmic electrodes were fabricated before the bonding experiments. For nonohmic contacts, the bonded wafer was cut into four  $4 \times 4$  mm specimens. One specimen was not annealed. The other three specimens were annealed at 200, 400, and 600°C for 1 h in air. The electrodes with conductive silver paste (2 mm diameter) for each specimen were made after bonding and annealing. Because the processing temperatures for the fabrication of ohmic contacts for GaAs and GaP were in between the annealing temperatures used for the investigation of the interfacial characteristics, we had to prepare nonohmic contacts after annealing the bonded specimens. This allows avoiding the heating influence on the interfacial behavior resulting from processing temperatures for ohmic electrodes.

Surface activation and surface roughness are two key parameters in SAB that were investigated using an X-ray photoelectron spectroscope (XPS) and an atomic force microscope (AFM, Seiko Instruments), respectively. The XPS spectra on the surfaces were taken by a Perkin-Elmer XPS using a monochromatic Mg  $K\alpha$  X-ray radiation source at 15 kV and 400 kW. Before surface activation, strong peaks of carbon and oxygen on both of the specimen surfaces were observed (Fig. 1). After 180 s into the surface activation, these peaks disappeared and activated the surfaces. Figure 1b shows that

\* Electrochemical Society Active Member.

<sup>z</sup> E-mail: mrhowlader@ece.mcmaster.ca

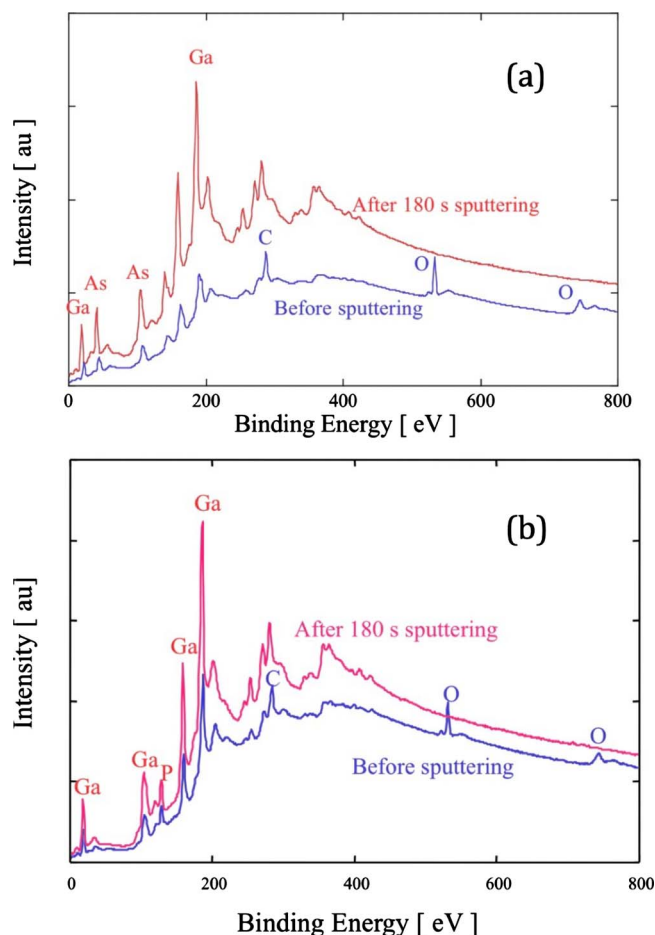


**Figure 1.** (Color online) XPS spectra for the activated surfaces of (a) GaAs and (b) GaP wafers compared with the nonactivated surfaces. The activation was done using a 1.5 keV Ar-FAB for 180 s.

the peak for P decreases with respect to that of the gallium in GaP after sputtering for 180 s. This indicates depletion of phosphorus in GaP after sputtering. The depletion of phosphorus is consistent to that of InP that was detected by a comprehensive XPS analysis.<sup>16</sup> Operated in a nonelectrode dynamic mode, the AFM measured the surface roughness over a scan area of  $3 \times 3 \mu\text{m}$ . Before surface activation, the rms surface roughness of GaP was 0.19 nm (Fig. 2). After surface activation, the value increased to 0.25 nm. Similar rms surface roughness results of GaAs have been reported in Ref. 17, which revealed an increase from 0.2 to 0.34 nm, 180 s after surface activation. Therefore, smooth activated surfaces were prepared to bond GaP/GaAs at room temperature.

For practical applications, high bonding strength is required to thin materials using chemical mechanical polishing.<sup>2</sup> Without annealing, the estimated average tensile strength of the specimens was 9.8 MPa. The fracture images of GaP and GaAs after the tensile test of the bonded wafers without heating showed a bulk fracture in GaP (Fig. 3). The bulk fractured GaP remained on the GaAs crystal after the tensile test. Due to the mesa structure of GaAs, the exterior area of the wafers was not bonded.

The  $I$ - $V$  characteristics of the p-GaP/n-GaAs bonded wafers were measured using a semiconductor parameter analyzer (model no. HP-4145B). The p-n junction current density increased as the applied voltage increased in both the specimens with ohmic and nonohmic electrodes, as shown in Fig. 4. The electrical current density was increased as the annealing temperature increased. Different breakdown voltages at different annealing temperatures were observed. In the forward bias, the threshold voltage with ohmic electrodes was

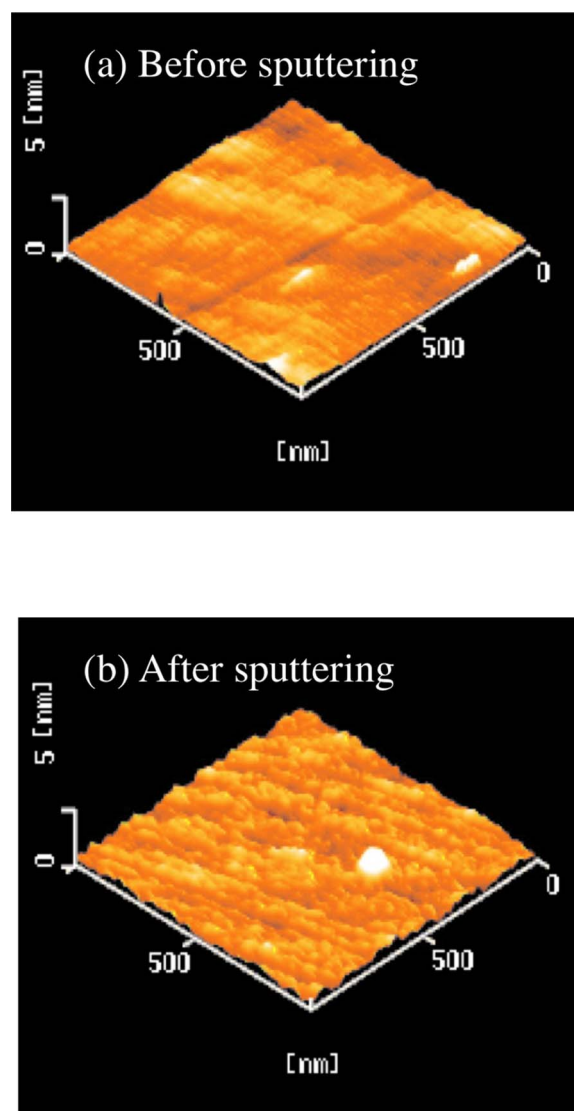


**Figure 2.** (Color online) AFM images of GaP surfaces (a) before and (b) after activation. The activation was done using a 1.5 keV Ar-FAB for 180 s.

less than 2 V. The breakdown voltage of the specimen annealed at  $600^\circ\text{C}$  increased to 5 V. The higher breakdown voltage is attributed to the higher voltage drop between the surface of the bonded wafers and the silver paste electrode. This observed behavior is different from the ones of the n-n and p-n GaAs interfaces, where a small portion of the voltage drops at the substrate. Most of the applied voltage drops across the depletion region at the interface have been reported.<sup>11,14</sup> In this study, the dependence of the breakdown voltage with annealing temperature was also observed. The reverse bias behavior showed that the higher the annealing temperature, the lower the breakdown voltages. The decrease in breakdown voltage due to reverse bias results from the annealing-induced change in defects and doping profiles at the bonded interface. The  $I$ - $V$  characteristics were further investigated by estimating the ideality factor and the barrier height using the following thermionic emission theory<sup>18</sup>

$$I = I_0 \left[ \exp\left(\frac{qV}{nkT}\right) - 1 \right] \quad [1]$$

where



(a) GaP



(b) GaAs

**Figure 3.** (Color online) Fracture images of (a) GaP and (b) GaAs surfaces after tensile pulling test of the GaP/GaAs bonded specimen.

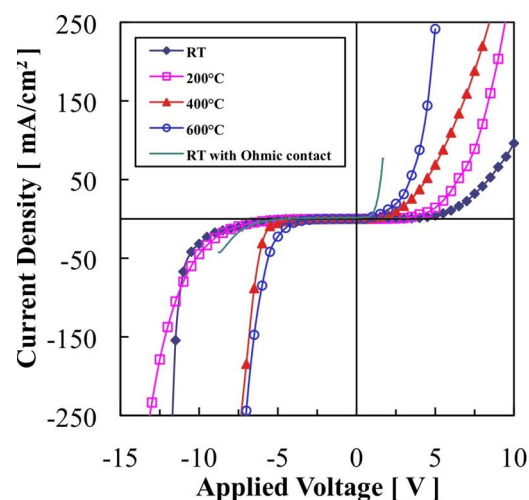
$$I_0 = AT^2 \exp\left(-\frac{qV_b}{kT}\right) \quad [2]$$

and

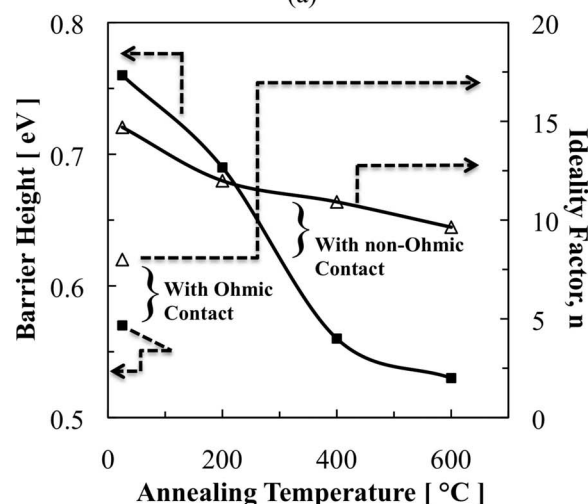
$$V_b = \frac{kT}{q} \ln\left(\frac{AT^2}{I_0}\right) \quad [3]$$

is the extrapolated value of a current density at a zero voltage,  $V_b$  is the barrier height,  $A$  is the Richardson constant,  $q$  is the electron charge,  $V$  is the applied voltage,  $k$  is the Boltzmann constant,  $T$  is the temperature in kelvin, and  $n$  is the ideality factor (assuming that  $A = 8 \text{ A/cm}^2 \text{ K}^2$  and  $T$  is 300 K).

Figure 4b shows the ideality factor and the barrier height for the ohmic and nonohmic electrodes. The estimated value for the ideality factor with ohmic electrodes was 8. The high ideality factor of GaP/GaAs may be attributed to a prolonged activation as well as to a high carrier concentration.<sup>16,17,19</sup> In contrast to ohmic electrodes, the ideality factor of the nonohmic electrode was higher. The higher ideality factor of the nonohmic electrode compared with that of the ohmic electrodes reflects the potential drop between the electrode



(a)



(b)

**Figure 4.** (Color online) (a) Current density and (b) ideality factor and barrier height of the p-GaP/n-GaAs interface with ohmic electrodes compared with nonohmic electrodes as a function of annealing temperatures. The specimen with ohmic contacts was not annealed.

and the substrate surface. The barrier heights and ideality factors were dependent on the types of electrodes. The ideality factor of the specimen with nonohmic contacts shrinks with the increase in annealing temperature. While the barrier height for the ohmic electrode was 0.57 eV, it was 0.75 eV for the nonohmic electrodes. The barrier heights for the nonohmic electrodes were decreased as the annealing temperature increased. The decrease in barrier height with the increase in temperature indicates a decrease in the interface defect states, which act as recombination centers for traps. The high ideality factor and the temperature-dependent barrier height can further be explained by the nanostructure of the bonded interface, as discussed below.

Figure 5 shows the nanostructure of the bonded GaP/GaAs interfaces. Without annealing, two amorphous layers with equal thicknesses of 3.5 nm were observed at the interface. It has been reported that the Ar atom implantation generates surface damage during activation, resulting in an amorphous layer at the interface.<sup>6</sup> The existence of amorphous layers across the bonded interface prohibits fracturing due to CTE mismatch while heating. Relative to the other direct wafer bonding interfaces, our interface had little to no voids.<sup>14</sup> Because it was relatively bonded in a UHV, there were no oxides across the bonded interface in contrast to the presence of amorphous

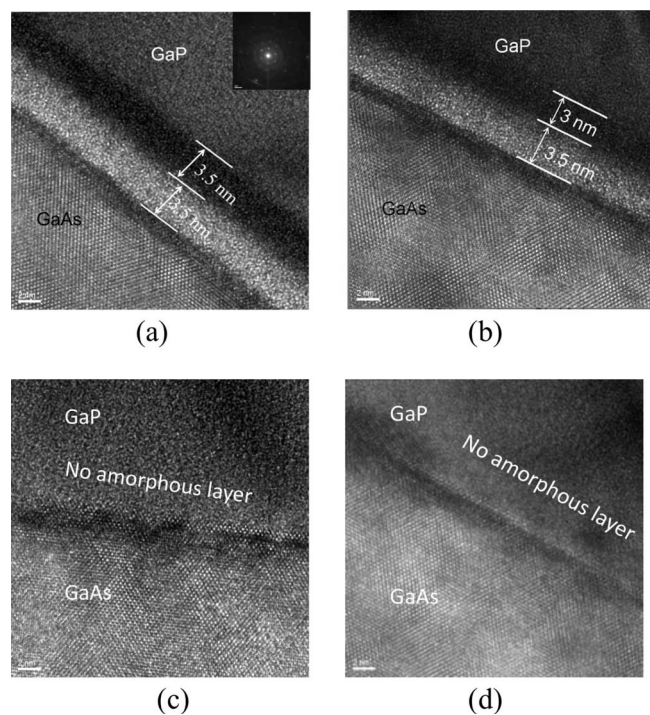


**Figure 5.** Nanostructure of GaP/GaAs bonded interfaces (a) before annealing and after annealing at (b) 200, (c) 400, and (d) 600°C. Annealing diminishes amorphous layers.

oxide layers at the n-n GaAs bonded interface using the hydrophilic bonding method.<sup>11,14</sup> The thickness of the amorphous layers adjacent to the GaP side was reduced from 3.5 to 3.0 nm upon annealing at 200°C. When the annealing temperatures were increased to 400 and 600°C, the amorphous layers diminished. Thus, the reduced amorphous layer thickness upon annealing is responsible for the observed improved *I-V* characteristics. This implicates fewer barriers for tunneling electron current. Therefore, the interfacial amorphous layers control the current transport of p-GaP/n-GaAs.

The production of amorphous layers as well as defect states induced by the Ar-FAB was simulated using SRIM version 2008.04. Figure 6 shows a comparative study of the Ar ions distributed in GaAs and GaP. The simulation parameters used were Ar atoms at 1.5 keV with an incident angle of 45° from the source with respect to the surface. The projected range of GaP and GaAs was 29 and 25 Å, respectively. The displacement threshold energy for GaAs is higher than that of GaP. While the same amount of energy is required to displace Ga and As atoms in GaAs, less energy is needed to displace P in GaP. As a result, this depletes the P atoms in GaP. This depletion is also reported when GaP and InP are treated with a 1.5 keV Ar-FAB and a 3 keV Ar ion.<sup>16,20</sup> Therefore, the amorphous layers adjacent to GaP across the interface are attributed to the Ga-rich layer due to the depletion of P.

In conclusion, p-GaP and n-GaAs wafers were bonded at room temperature by the SAB method, and the influence of thermal cycles on the characteristic behavior of the bonded interface was demonstrated. The bonding strength was 9.8 MPa measured by the tensile pulling test. Two amorphous layers with identical thicknesses of 3.5 nm were found across the interface without annealing. Annealing improved the electrical *I-V* characteristics and reduced the amorphous layers across the interface. The amorphous layer adjacent to

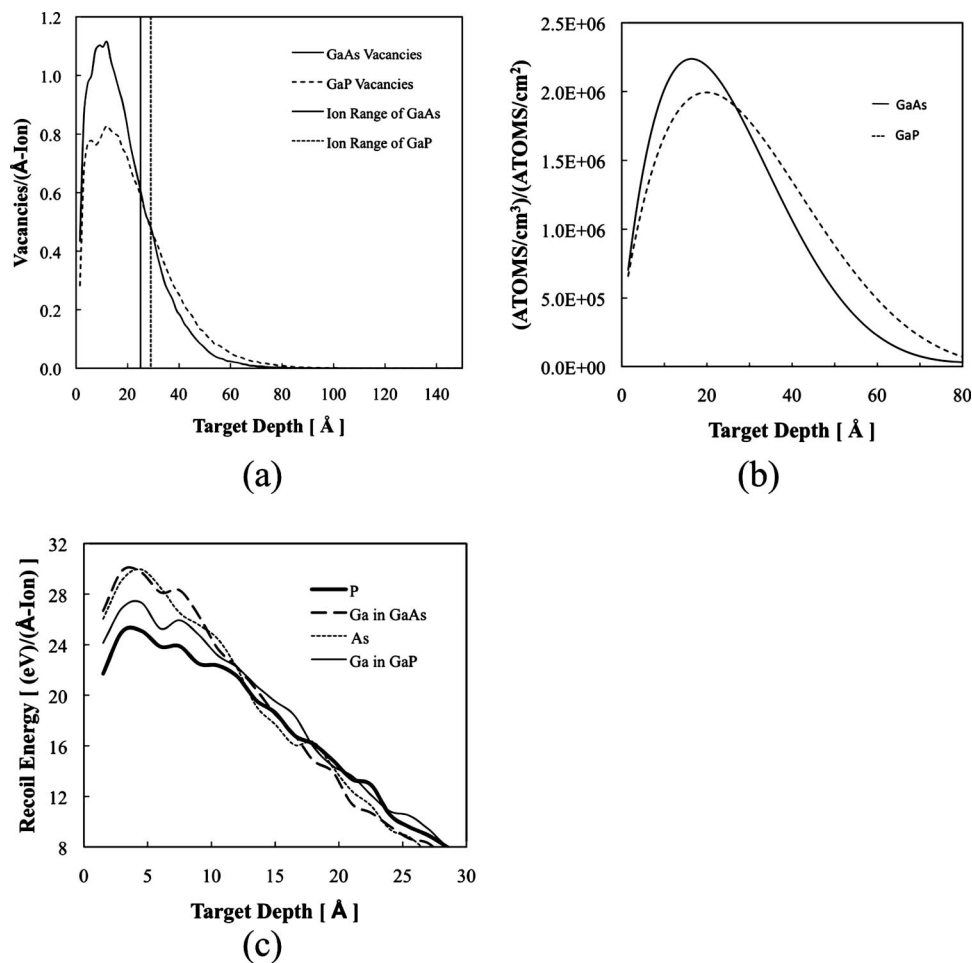


**Figure 6.** Distribution of Ar ions in terms of (a) vacancies per angstrom length per ion, (b) density of atoms over fluence, and (c) recoil energy in electron volt per angstrom per ion as a function of depth in GaAs and GaP.

GaP across the interface is attributed to the Ga-rich layer due to the depletion of P. This room-temperature bonding not only applies to devices that cannot withstand higher temperatures, but also improves the performance of devices that may be exposed at higher temperatures during the fabrication process flow.

#### Acknowledgments

Kyle Cormier at McMaster University is acknowledged for the simulation work. Professor C. Kinoshita and Professor K. Yasuda of Kyushu University, Japan are greatly appreciated for their valuable opinion on the SRIM results.

*McMaster University assisted in meeting the publication costs of this article.*

#### References

1. F. A. Kish, F. M. Steranka, D. C. DeFevere, D. A. Vanderwater, K. G. Park, C. P. Kuo, T. D. Osentowski, M. J. Peanasky, R. M. Fletcher, D. A. Steigerwald, et al., *Appl. Phys. Lett.*, **64**, 2839 (1994).
2. C. K. Lin, S. W. Ryu, W. J. Choi, and P. D. Dapkus, *IEEE Photonics Technol. Lett.*, **11**, 937 (1999).
3. L. C. Olsen, X. Deng, W. Lei, F. W. Addis, and J. Li, in *The 25th IEEE Photovoltaic Specialists Conference*, IEEE, p. 61 (1996).
4. A. A. M. Farag, F. S. Terra, and G. M. Mahmoud, *Sens. Actuators, A*, **150**, 231 (2009).
5. Z. R. Huang, D. Guidotti, L. Wan, Y.-J. Chang, J. Yu, J. Liu, H.-F. Kuo, G.-K. Chang, F. Liu, and R. R. Tummala, *IEEE Trans. Compon. Packag. Technol.*, **30**, 708 (2007).
6. H. Takagi, R. Maeda, N. Hosoda, and T. Suga, *Jpn. J. Appl. Phys., Part 1*, **38**, 1589 (1999).
7. T. Suga, *Ind. Ceram.*, **19**, 176 (1999).
8. T. R. Chung, L. Yang, N. Hosoda, H. Takagi, and T. Suga, *Appl. Surf. Sci.*, **117-118**, 808 (1997).
9. J. Geske, Y. L. Okuno, J. E. Bowers, and V. Jayaraman, *Appl. Phys. Lett.*, **79**, 1760 (2001).
10. N. Liu and T. F. Kuech, *J. Electron. Mater.*, **36**, 179 (2007).
11. F. Shi, S. Maclaren, C. Xu, K. Y. Cheng, and K. C. Hsieh, *J. Appl. Phys.*, **93**, 5750 (2003).
12. P. C. Liu, C. L. Lu, Y. S. Wu, J. Cheng, and H. Yang, *Appl. Phys. Lett.*, **85**, 4831 (2004).
13. N. Razek, A. Schindler, and B. Rauschenbach, *Vacuum*, **81**, 974 (2007).
14. F. Shi, K. Chang, J. Epple, C. Xu, K. Y. Cheng, and K. C. Hsieh, *J. Appl. Phys.*, **92**, 7544 (2002).
15. T. Akatsu, A. Plossl, R. Scholz, H. Stenzel, and U. Gosele, *J. Appl. Phys.*, **90**, 3856 (2001).
16. M. M. R. Howlader, T. Watanabe, and T. Suga, *J. Appl. Phys.*, **91**, 3062 (2002).
17. M. M. R. Howlader, T. Watanabe, and T. Suga, *J. Vac. Sci. Technol. B*, **19**, 2114 (2001).
18. *Heterojunction Band Discontinuities*, F. Capasso and G. Margaritondo, Editors, Chap. 8, North-Holland, Amsterdam (1987).
19. H. Wada, Y. Ogawa, and T. Kamijoh, *Appl. Phys. Lett.*, **62**, 738 (1993).
20. W. Yu, J. L. Sullivan, S. O. Saied, and G. A. C. Jones, *Nucl. Instrum. Methods Phys. Res. B*, **135**, 250 (1998).